Sensors & Transducers, Vol. 228, Issue 12, December 2018, pp. 48-62

www.sensorsportal.com

Sensors & Transducers

Published by IFSA Publishing, S. L., 2018
http://www.sensorsportal.com

Nanostructure Protein Toroidal Array Devices Promoted Room Temperature Superconductivity and Direct Sensing of Collagen-1

[1] E. T. CHEN, [2] J. T. THORNTON, [3] P. T. KISSINGER, [4] S.-H. DUH

[1] Advanced Biomimetic Sensors, Inc., 11140 Rockville Pike, Suite 440, Unit 422, Rockville, MD 20852, USA
[2] Bruker Nano, 19 Fortune Dr., Billerica, MA 01821, USA
[3] Department of Chemistry, Purdue University, West Lafayette, IN 47906, USA
[4] University of Maryland Medical System, 22 South Greene St, Baltimore, MD 21201, USA
Tel.: 240-706-5687, fax: 240-630-4051
E-mail: ellenchen@nanobiomimeticsensors.com

Received: 11 June 2018 /Accepted: 1 October 2018 /Published: 31 December 2018

Abstract: Two types of superconductive/memristive devices were developed based on a protein Matrix Matelloproteinase-2 (MMP) cross-linked polymer toroidal membrane and a biomimetic multiple-layered super lattice organo-metalic membrane. Cooper pair's two-wave sounds were "heard" in the Josephson toroidal junction using the Open Circuit Potential method. The rate constant for the exponential voltage decay curve of the innate protein device is 122-fold higher than that of the biomimetic device. Sine wave phase change and oscillating curves were observed at 1 and 10 kHz for multiple scan cycles, with peak intensity kept constant on the innate protein device compared with the biomimetic device. The quantum conductance density of the biomimetic device is 3.1×10^{10}-fold higher than the activated protein device at 1 Hz. The protein devices were able to direct detect collagen -1 at the innate and activated state. The biomimetic device has a wider analytical range and higher sensitivity compared with the protein device.

Keywords: Protein Made Nanostructure Toroidal Circular-accelerator Array; High Frequency Innate Protein Oscillator and Superconductor; Room Temperature Organo-metal superconductor; Nanobiomimetic MMP-2 Superconductor; Superlattice; Josephson Junction; Superconducting and Sensing Device; Probe-free and Label-free.

1. Introduction

Collagen is the primary structural component of the extracellular matrix (ECM) that is responsible for physical maintenance of all cells [1]. The triple-helical structure of collagen assembles into insoluble collagen fibrils to strengthen the bones and tissues preventing proteinase from engaging [1-2]. Collagen is a double edged sword not only does it actively pave the road for physiologically normal cell and pathologically abnormal cell adhesion, migration and intracellular communication, but also it activates some receptors for either the over-production of or the failure of the matrix; this degradation is cased by either bacterial collagenase or abnormal fibrosis from fibroblast cells, endothelial cells or epithelial cells, and hence many diseases are associated with the malfunction of collagen [1-5]. A long history of

traditional approach has been used based on denaturing collagen as a substrate to probe collagen degradation or to study matrix matelloproteinase (MMP) activity [6-7]. However, a clinically useful detection range at the low end for collagen-1 is difficult to accomplish due to the denaturing process.

The Josephson coupled-superconductor effect is inherent in many superconductor-insulator-superconductor (S-I-S) tunnel junctions if the two sides of barriers are sufficiently thin to allow the coupling energy from the cooper pair tunneling at the coherent wave state between the two superconductors to exceed thermal fluctuations [8-10]. Inspired by several reports and predictions [11-13], we thought the unique coherent wave state produced in the S-I-S module at a toroidal Josephson junction may be a key feature to help accomplishing the goal of this project, where we attempt to utilize a circular JJ to solve our biosensing problem. Inspired by another theoretical prediction of a π-phase difference on a topological-superconductor (TSC)/normal metal (NM) can arise, induced by Majorana spin-triplet paring, which exhibits a Josephson phase of 0 and π-junction in its ground state without any applied magnetic flux [12].

Inspired by our prior published literature in developing a nanostructure biomimetic Matrix Metalloproteinase-2 (MMP-2) superconductive, memristive, memcapacitive and meminductive device for sensing fg/mL collagen under antibody-free and reagent free conditions by utilizing an approach that used collagen as an analyte and also used it as an unique Josephson toroidal junction barrier to promote Direct Electron-Relay (DER) in a superlattice organo-metal membrane [14-15] at an innate state without denaturing the protein.

This report is to further explore the nature of the protein MMP-2 superconductive/memristive device and answer the questions of why this device can promote superconductivity and direct detecting low concentration collagen possible at room temperature without a reagent was used. Our approach was to build two superlattice devices; the biomimetic device was made of double-layer biomimetic MMP-2 material membranes by cross-linking the conductive polymers and zinc ions embedded. The protein device was made of protein MMP-2 cross-linked with the same conductive organic polymer forming a single-layer toroidal array without adding zinc ions. We used the collagen as an analyte and acted as a dielectric barrier in the Josephson junction. The zinc ions are also acted as the Josephson junction barriers. The focus of this report is to compare the two devices' kinetic behavior in accelerating Cooper pairs' transpassing the Josephson barrier at zero-bias at room temperature without external magnetic field applied, and no radio frequency power supply is needed in the presence of collagen compared without collagen. Because the biomimetic device does not contain protein cysteine, its function is to mimic the "activated" state protein MMP-2.

Recent theoretical predictions of Josephson-based meminductive, memristive quantum susperconducting devices have drawn an attention [16-18] that the Josephson super current behaves hysteretically. We proposed to develop a TSC/quantum memristor (QMR) or a TSC/quantum memcapacitor (QMC) device that is able to direct measure collagen in a biological sample without denaturing the protein under a reagent-free conduction. It is well known that superlattice membranes have been used as candidates for applications in superconductivity [19], wherein developing superlattice membranes with unique materials and compositions were our priority.

2. Results and Discussions

2.1. Evaluation of the Friedel-oscillation in the Superlattice Membrane

The morphology of the AU/SAM was characterized using an Atomic Force Microscope (AFM) (model Dimension Edge AFM, Bruker, MA). Data was collected in TappingMode using silicon probes with 5-10 nm tip radius and ~300 kHz resonance frequency (Probe mode TESPA-V2, Bruker, MA). Evaluations of the Friedel-oscillation on Device 1 were conducted based on the AFM images. Friedel-oscillation is a phenomenon of long-range indirect interactions between electrons on the surface [18]. The AFM images of the biomimetic device are depicted in Fig. 1A with 3D view of the curvature of the single-wall nanotube with a zinc atom, and Fig. 1B is the 2D view of the superlattice with the zinc atoms having the Friedel-oscillation in the center zinc atom. Fig. 1C depicts a whole screen shot image of the membrane of Device 1 before the AFM image was taken. Fig. 1D depicts the first superconducting layer in a 3D view of nanoisland. Fig. 1E depicts the nature MMP-2 sensor's single-wall nanotubule toroidal structures with zinc atoms that look like diamonds on a ring. All rings have the same thickness in 90 nm in the circular nanotubes, and the diameters of the toroidals are in the range of 2.3-5.5 μm, and the height of the toroidal is from 0.5 to 0.9 μm. The Friedel-oscillation was observed as the zinc atoms oscillate on the edge or in the center of the ring. Zinc atom migration from the original cluster to other rings was observed. Fig. 1F depicts the superlattice toroidal array in the Height sensor mode of the AFM of the protein membrane in 1 μm^2.

2.2. An Engineering Design of the Devices

The art module of the protein device presented in Fig. 2A shows the engineering design the toroidal nanostructure cross-linked with polymers. The metal atoms in the MMP-2 play an important role as flexible Josephson junction barriers that interact with the collagen dielectric barrier. Fig. 2B shows the toroidal structure of the protein cross-linked polymer membrane. Fig. 2C shows the engineering design of the biomimetic device with the art model in a side

view of the Josephson junction. The cyclodextrin array matrix was in alignment in three dimensions and produced the eternal non-ferromagnetic field. The nano-island membrane on the gold electrode was at the bottom with the superlattice membrane on the top. The wave of Cooper pair electrons after passing through the nano-island membrane then passed the zinc atom barriers, and finally they passed the collagen barrier, which is a dielectric barrier.

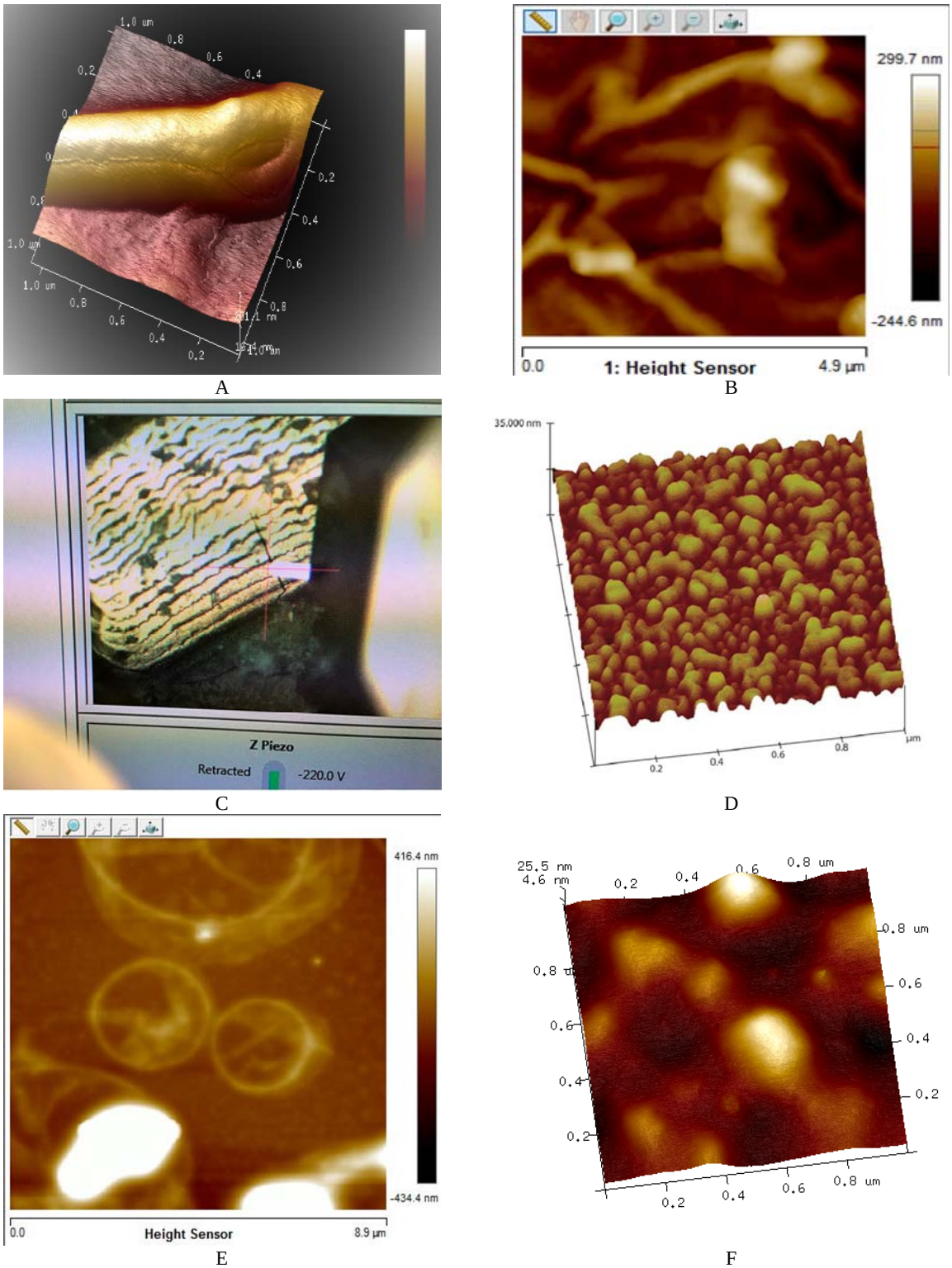

Fig. 1. (A) Biomimetic device 's surface structure in 3D view of the curvature nanotube. (**B)** 2D view of the superlattice with zinc atoms. (**C)** Biomimetic device's whole screen shot image before the AFM image was taken. (**D)** First superconducting layer in a 3D view of nanoisland. (**E)** Nature MMP-2 device circular structures with zinc atoms. (**E)** Tapping mode for detail shown the zinc atoms in the nature MMP-2 protein membrane and (**F**) is the AFM in Height sensor mode.

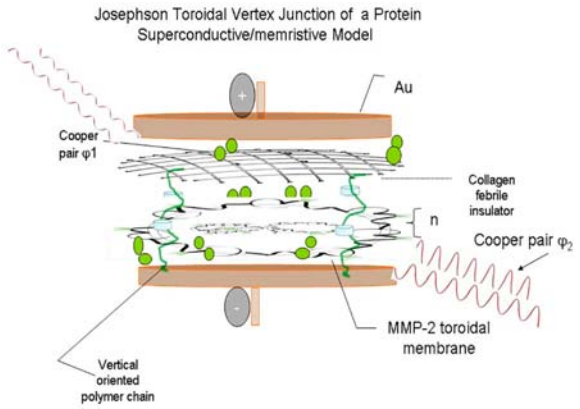

Fig. 2A. Engineering design of the protein device with the toroidal nanostructure membrane. The metal atoms in the MMP-2 play an important role as flexible Josephson junction barriers that interact with the collagen dielectric barrier.

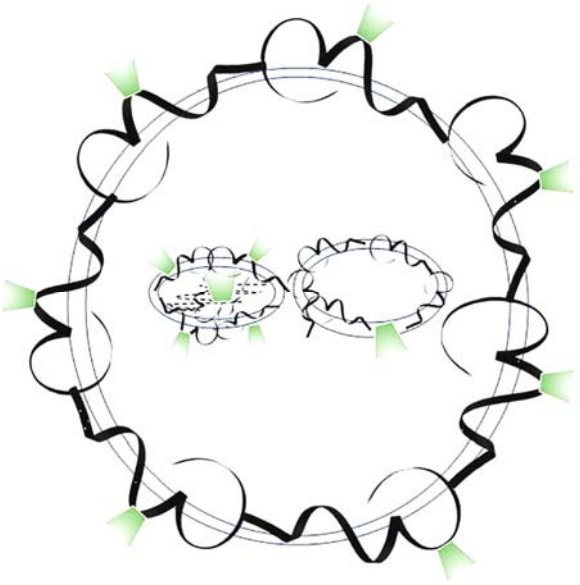

Fig. 2B. Shows the toroidal structure of the protein cross-lined polymer membrane. The zinc atoms are diamonds on the ring.

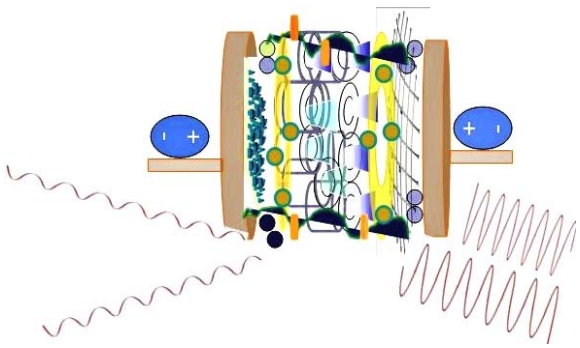

Fig. 2C. Biomimetic device with the art model in a side view of the Josephson junction.

3. Transformation from the Memristive State to Superconductive State

3.1. The Transformation from Memristive to Superconductive Between the Innate and Activated States of the Protein Device

The scan rate affected on the current intensity of the innate protein device in PBS solution demonstrated by the CV method that the device has an abnormal memristive characteristics as shown in Fig. 3A. The Direct Electron Transfer $(DET)_{red}$ peak current intensity increased exponentially as the scan rate increases from 1 Hz to 10 kHz. The first-order exponential decay model fitting results shown in Fig. 3D indicate both, the DET_{red} and DET_{ox} vs. scan rate does not follow the typical memristive curve behavior which is that the peak intensity will be reduced when the scan rate increased to the highest [20]. In contrast, both curves are in an exponential increase or decrease manner and reached the s-s state at 10 kHz, and the DET_{ox} curve's rate is only higher than the DET_{red} curve by 7 %. This is a strong evidence of the existence of a circular accelerating vortex force that changed the memristivity to a sine wave oscillating nature at the higher frequency scan as shown in the curve at 10 kHz in Fig. 3A. Fig. 3B depicts the activated protein device had the JJ tunneling supercurrent occurred at very low scan frequency 1 Hz and to high frequency at 1 kHz and 10 kHz at zero-bias, respectively. Fig. 3C shows the current intensity changes between DET_{red} and DET_{ox} peaks over scan frequency (1 to 10 kHz) between the innate and the activated state, respectively. The activated state of the protein device has a 50 and 10-fold increase in current intensity compared to its innate state for DET_{red} and DET_{ox}, respectively.

3.2. Kinetic Study in the Josephson Toroidal Array Junctions

This Section is to report the results obtained in the kinetic study using the CV method by scan the potential from 0.8 V to -0.8 V by 10 cycles of consecutive scans at a higher scan rate 300 Hz, 1 kHz and 10 kHz, respectively in the Josephson toroidal array junctions compared to the results between the innate protein device and the biomimetic device in PBS solution. At zero-bias potential, there is a negative supercurrent observed at 300 Hz scan rate for the innate protein device as shown in Fig. 4A. The hysteresis point far from origin was observed. There are many oscillation sine waves observed in Fig. 4B that included the origin located in the curve envelop. There was no peak intensity change observed in the 10 scan cycles. Fig. 4B shows a significant event happened that in the first forward scan, the **sine** wave has an absolute peak height of 1.592 nA and the λ length within the adjacent peak is

0.0114 V; the backward scan has a **cosine** wave with an absolute peak height of 1.56 nA and the λ value is 0.0166 V. As the scan cycle increases, the peak location has a small movement toward to the lower field by 0.9 mV for each consecutive cycle and the overall peak intensity did not change over the entire scan range. For a clear view, Fig. 4B only shows the range between 0.06 V to -0.06 V. Fig. 4C depicts the forward **sine** wave and the backward **cosine** wave has similar peak height of 11.42 nA and the between peak λ value is 0.1643V over 0.06 V to -0.06 V at 10 kHz for 10 cycles at 10 kHz. Fig. 4D shows the 10 kHz wave over -0.8 to 0.8 V. The peak height kept unchanged and the only change was the phase change that indicates the innate protein device at 10 kHz high frequency becoming a strong oscillating circular accelerator kept periodic phase changes without energy dissipation at zero-bias potential. We observed an opportunity for quantum computing exists for "+1", "0" and "-1" at zero-bias can be occurred simultaneously as shown in Fig. 4B, Fig. 4C and Fig. 4D. The superconductivity at zero-bias also observed in these figures. Without the presence of collagen, only the presence of the circular oscillation phenomena based on the super lattice ring structure could provide enough attractive forces that pave the road for direct sensing of collagen without using denaturing step, which is significant benefit. Its potential applications will be further exploded.

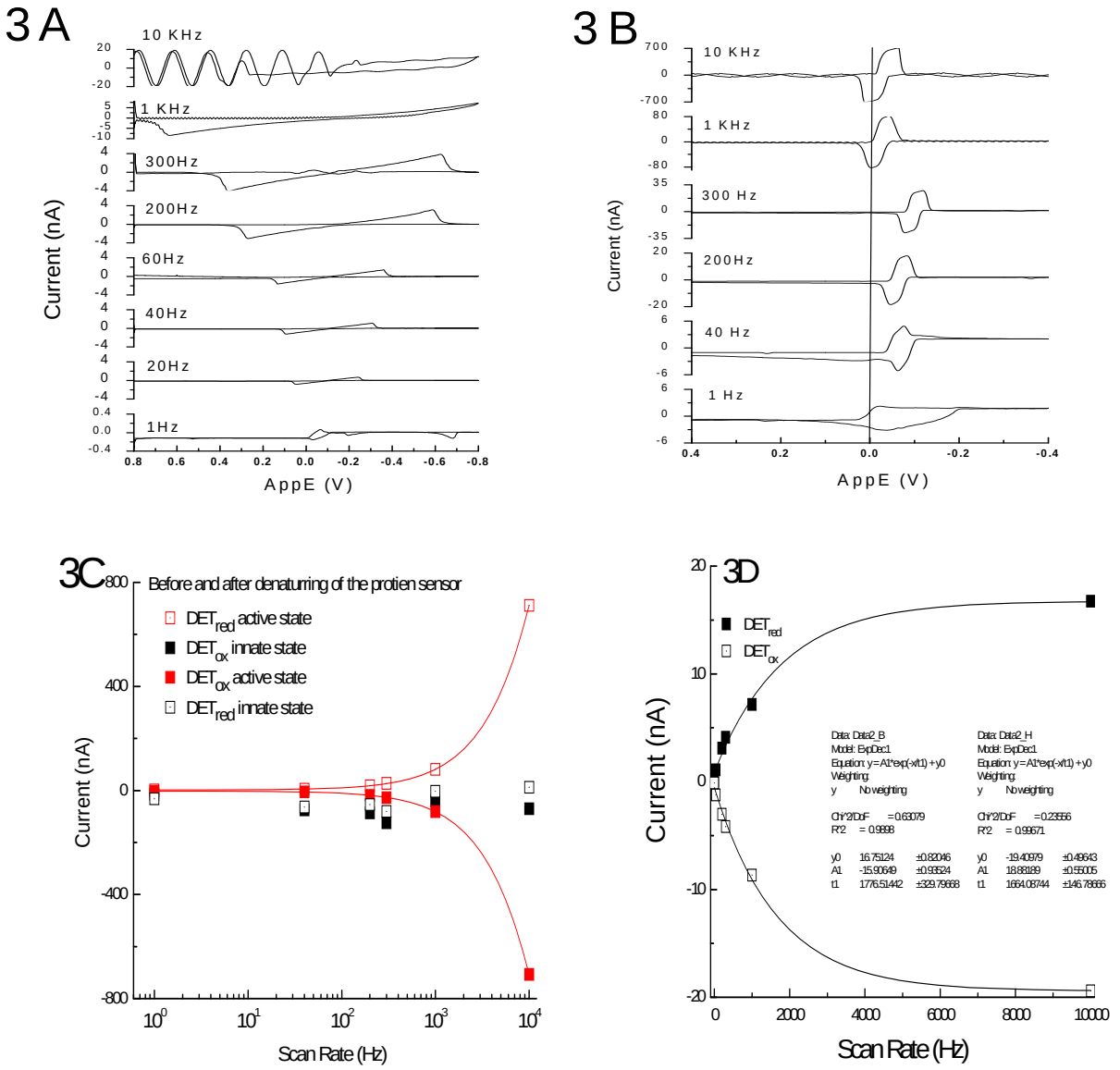

Fig. 3. (A) Scan rate impacts on **CV** curves **of** the innate protein Device in PBS solution. (**B)** Scan rate impacts on **CV** curves of the activated protein device in PBS solution. (**C)** Plots comparison of current vs. scan rate at the innate and the activation status of the protein device. (**D)** Current vs. scan rate of peak DET_{red} compared with peak DET_{ox} and the fitting curves.

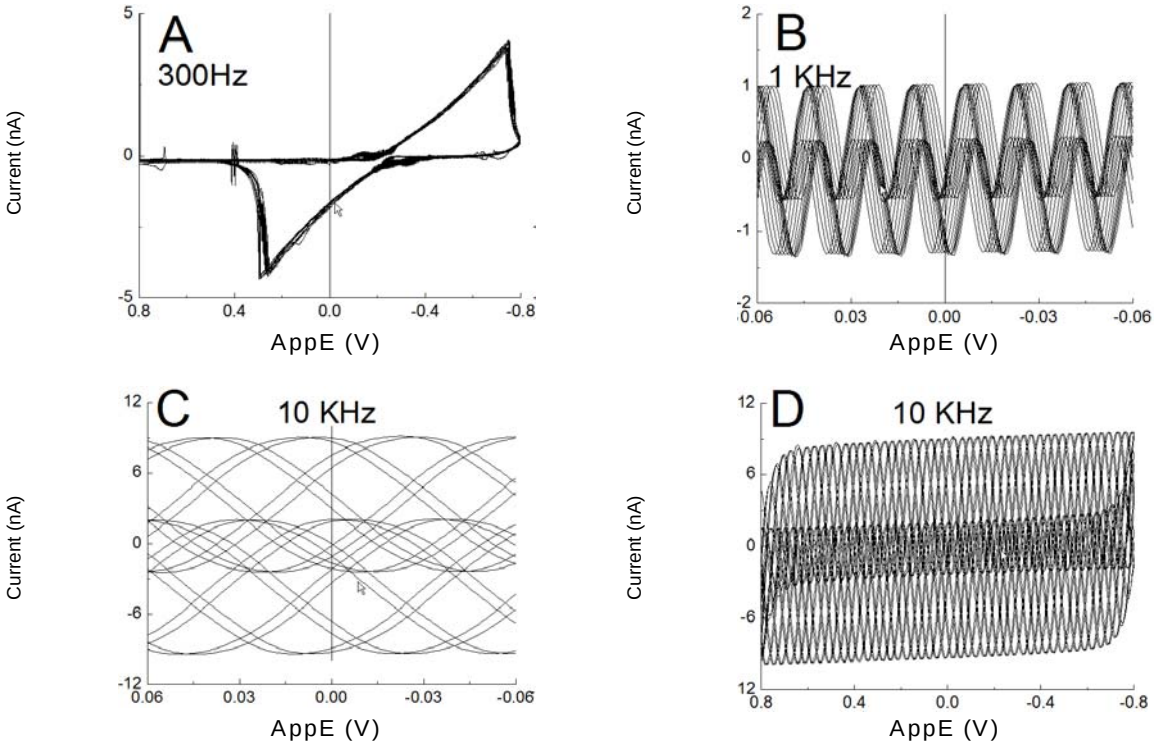

Fig. 4. (A) i-V curves for 10 consecutive scan cycles at 300 Hz for the innate protein device in PBS solution. (**B)** i-V curves of 10 cycles at 1 kHz. (**C)** shows the i-V curves of 10 cycles at 10 kHz. (**D)** shows the i-V curves over 0.8 V to -0.8 V at 10 kHz.

The highest DET_{red} and DET_{ox} peak intensity was observed under 300 Hz scan rate compared to higher scan rate 1 kHz and 10 kHz, which has lower intensity for the biomimetic device as shown in Fig. 5A. The current increase rate is proportional to the scan cycle number increase was also observed compared with Fig. 5B and Fig. 5C, respectively. The linear rate results of DET_{red} and DET_{ox} peak current vs. total 10 scan cycles are 0.02 mA/s and -0.04 mA/s for DET_{red} and DET_{ox}, respectively. The biomimetic device offers a higher rate at 300 Hz compared with the innate protein device having no such advantage. However, at higher scan rate up to 10 kHz, the innate protein device has the highest current with the strongest circular oscillation compared with the biomimetic device.

3.3. Study of the Cooper Pairs' Two-Wave Kinetics in Electron Magnetic Flux

The hallmarks of the JJ characteristics are (1) at a DC voltage = 0, an super current

$$I_s = I_c \sin(\triangle\varphi), \quad (1)$$

where I_c is the critical current, $\triangle\varphi$ is the phase difference between the waves of two superconductors, appears at the DC Josephson junction; (2) at a finite DC voltage, the phase of the super current is change vs. time that caused oscillating at the AC Josephson Junction, which is proportional to 2 eV_{DC}, i.e. [8],

$$\partial\varphi/\partial t = (2e/h)V_{DC} \quad (2)$$

Open circuit potential (OPO) method was used to study the Cooper Pair's two-wave transmission kinetics [8]. So far has no report shown regarding this observation, but it was predicted by B. Josephson several decades ago, that we should be able to see the Cooper Pair's second wave and hear its sound [8]. Our approach was to set up an experiment under open circuit potential condition, and record the wave's voltage either increase or decrease as time elapses; if indeed there is a second wave of the Cooper pair exists, it will show up spontaneously and randomly. The problem is that we do not know when and how it will show up. There are two curves shown as "a" for the voltage exponential increases as time increase with a first-order rate of $0.01\ s^{-1} \pm 3\times10^{-5}\ s^{-1}$ compared with the "flip" wave "b" of the Cooper pair rate constant of the exponential decrease of $1.22\ V.s^{-1} \pm 5\times10^{-5}\ V.s^{-1}$ as shown in Fig. 6 for the innate protein device in PBS control solution. There is a 122-fold rate results difference among the two waves. The signals at the s-s state have 8-fold difference that is a direct evidence of "Hearing" of the two-wave sounds from the Cooper Pair magnetic flux. The intrinsic electro-relay system within the toroidal cavities is activated under a zero-current open circuit condition, which is the driving force of the electromagnetic flux strength.

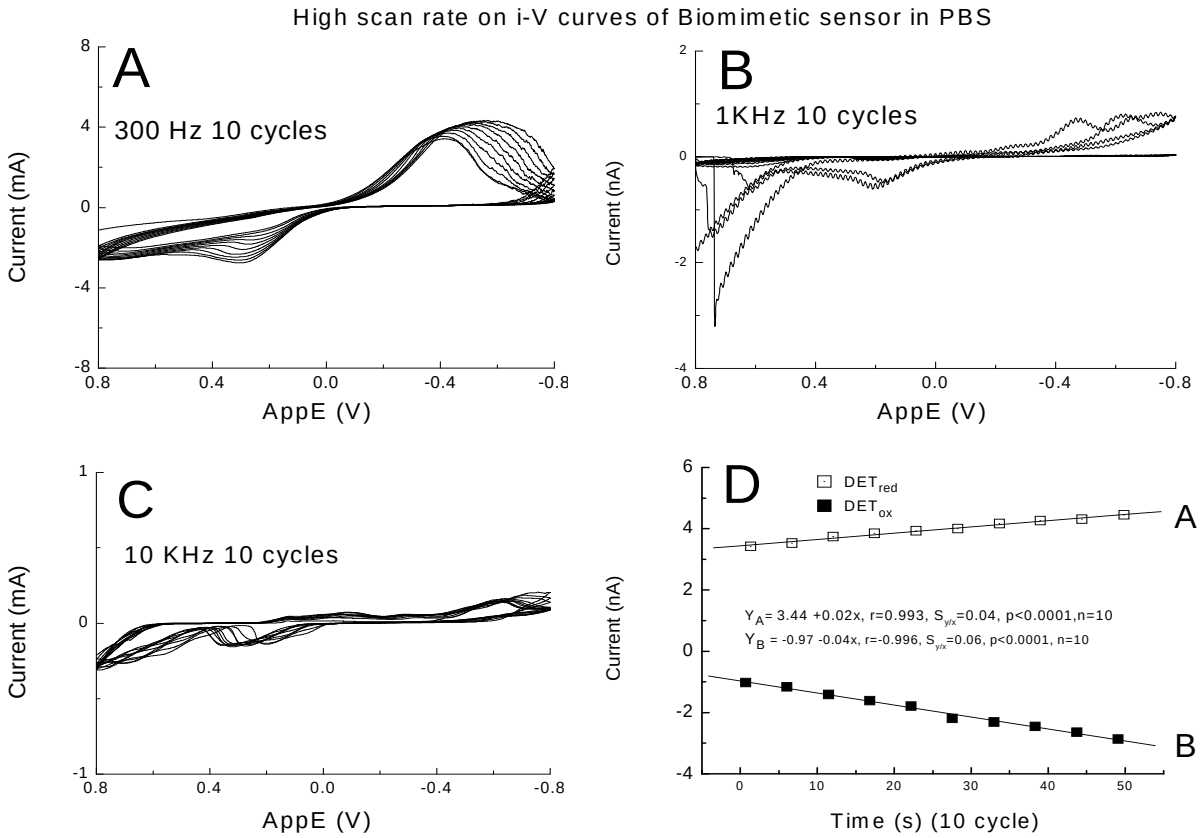

Fig. 5. i-V curves of biomimetic device in PBS solution at 300 Hz (**A**), 1 kHz (**B**) and 10 kHz (**C**) for 10 consecutive scan cycles, respectively. (**D)** Plots of current vs. time for DET_{red} and DET_{ox} peak in (**A).**

Fig. 7 depicts the Cooper Pair's non-linear amplification of increase potential in the tunnel of Josephson junction using the same OPO method for the biomimetic device in pure water and in pH 7.4, 10 mM PBS solution, respectively. Curve "a" exhibits an first-order exponential decrease rate of 0.01 ± 0.0001 V.s^{-1} in pure water; curve "b" and "c" in pure water and in PBS has the first-order exponential increase rate of 0.02 ± 0.003 V.s^{-1} and 0.014 ± 0.002 V.s^{-1} for in water and in PBS, respectively. The peak voltage between curve a, b and c has no significant difference at s-s state; but at the beginning of the discharge there is a 37-fold large difference between curve a and b or between a and c. The rate between the increase and the decrease curve is 30 % higher in pure water than in PBS solution. The Cooper pair coherences tunneling within the barrier and then suddenly degeneration happened, that caused a high open circuit potential occurred. That means the intrinsic waves are able to penetrate the Josephson junction barriers, such as zinc atoms. The biomimetic device offered advantage for quantum computing, because its 122-fold slower decrease rate than the innate protein device, i.e., it has a longer time stayed in the junction than the protein device, which enhances the memory storage. The design of the biomimetic device in emphasizing of the DER effect, multiple layers with superlattice structure, has gained the benefit for sensing, it will present in the late Chapter.

4. Comparing Various Step Time Effects on the Phase Change and Intensity

Comparing step time effects on the phase change and peak intensity between the two devices in PBS solution at zero-current was conducted by using the Double Step Chronopotentiometry method (DSCPO), i.e., the voltage method. The spontaneous sine wave electromagnetic flux discharge curve shows at 25 ms step time in Fig. 8B has the highest peak current than any other step times, and the sine wave was changed its phase in other step times as shown in the innate protein device in Fig. 8(A, C and D), respectively. The peak current in Fig. 8B is also 18-fold higher than in Fig. 9B of the Biomimetic device at 25 ms with a cosine wave. At 4 ms, the peak current is 22-fold higher in the protein device than with the Biomimetic device as shown in Fig. 9A indicates the innate protein device has high frequency advantage in circular accelerating. Fig. 9(C and D) at 4 s and 25 s step time does not offer significant advantage compared with the protein device.

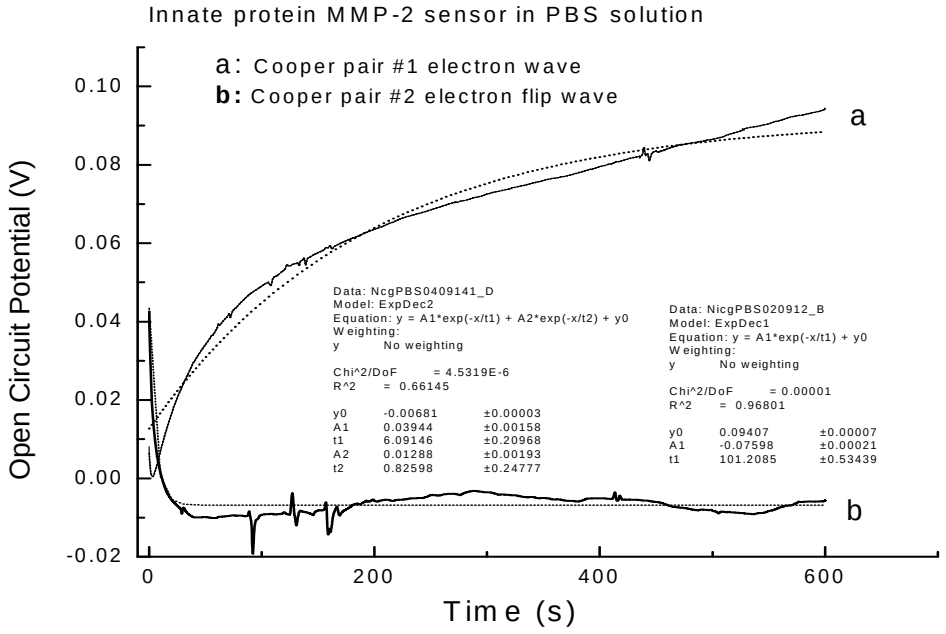

Fig. 6. Curves in open circuit potential for the innate protein device in the PBS solution.

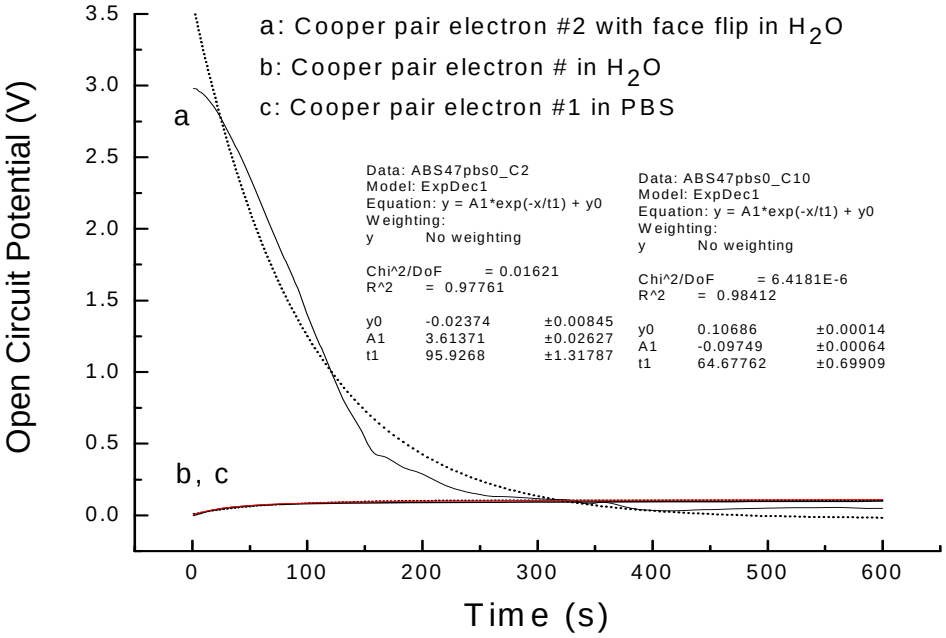

Fig. 7. Curves in open circuit potential for the biomimetic device in water (curve a) and in water and PBS (curve b and c).

5. Superconductivity

5.1. The JJ Curve's Characteristics

Fig. 10 shows the amplitude of the JJ super AC current from the biomimetic device is 9.5-fold higher than that of the innate protein device under zero-potential condition with peaks oscillating at 10 kHz using the Double Step Chronoamperometry method (CA) method. This means at zero-potential, there was no magnetic flux phase change, it has restricted the protein device, hence the biomimetic device's long range DER advantage shows up, which is a known electron pop-hop transport phenomena between the transition metal zinc and the d_π from polymer receptors [21-22], i.e., Cooper pairs quantum transport their electrons which are exchanged with holes of the receptors in the superlattice membrane.

As Liao mentioned in his report, zinc metal coordinates well with the tetraphenylporphine nitrogen atoms better than Fe, Co, Ni and Cu, because zinc's $d_{x2—y2}$ orbital energy significantly dropped, in favor of coordination with the d_π, i.e., π-cation radical, hence our experiment supports his finding that the d_π orbital may dominate the electron relay [23].

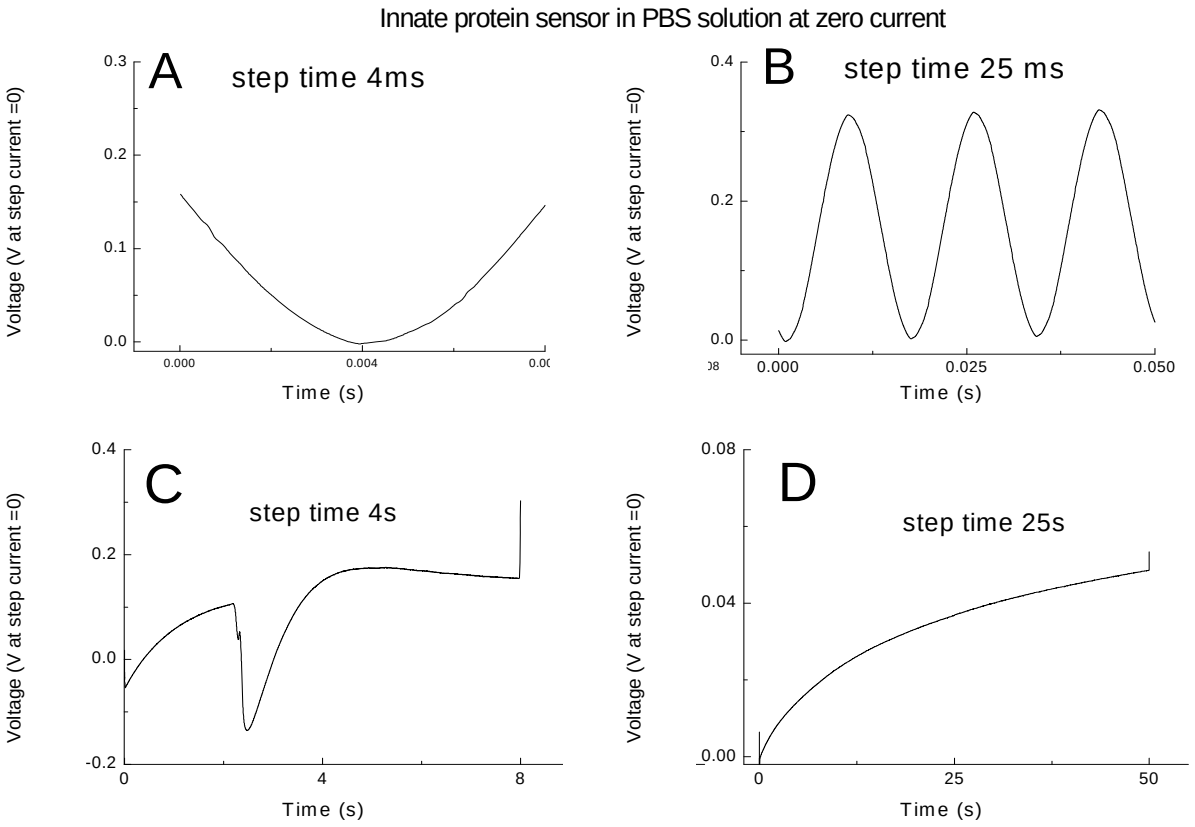

Fig. 8. Spontaneous electromagnetic flux discharge curves in step time 4 ms, 25 ms, 4 s and 25 s for the innate protein device in Fig. 8(A, B, C and D), respectively.

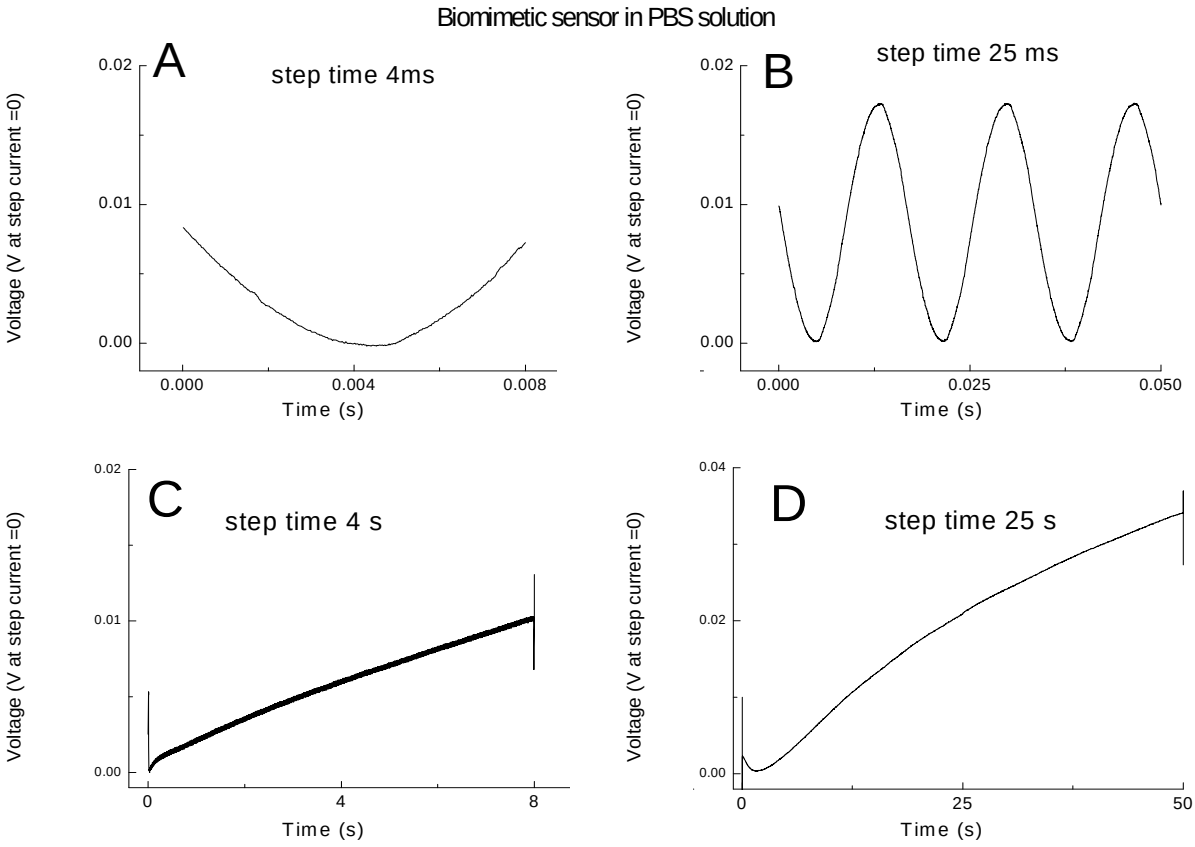

Fig. 9. Spontaneous electromagnetic flux discharge curves in step time 4 ms, 25 ms, 4 s and 25 s for the Biomimetic device in Fig. 9(A, B, C and D), respectively.

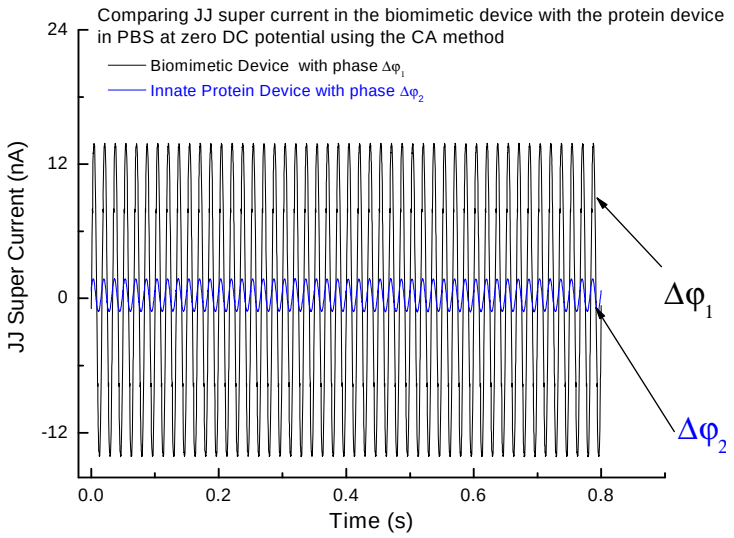

Fig. 10. AC current oscillating with time compared with the Biomimetic device and the innate protein device at the zero potential condition in PBS solution using the CA method.

5.2. Quantum Conductance

The biomimetic device utilized the first bottom layer of biomimetic Choline Acetyltransferase (CHAT) as the pseudo topological-superconductor (TSC) layer under the assumption that direct super JJ circular current flow will be promoted by the presence of collagen-1, and with the top layer of - bM-β-DMCD/TCD/PEG/PVP/$ZnCl_2$, - an activated biomimetic 3D collagen-1...MMP-2...CHAT relay tunnel may form a SIS/SIN device with the TSC/Quantum Memristor (QMR) function peak at zero-potential. Because the CHAT regulates the MMP-2 function and activity [24], in Fig. 11A, it was revealed that the JJ super current greatly increased at zero-potential compared with the control as shown in the insert with the hysteric i-V curve. Fig. 11B depicts the quantum conductance density per superlattice in the presence of collagen which is 34-fold higher compared with the control. The biomimetic device's quantum conductance density per superlattice is 3.1×10^{10}, 13 and 1.33-fold higher than that of activated protein device at 1 Hz, 1 kHz and 10 kHz, respectively as shown in Fig. 12A based on curves displayed in Fig. 3B. Activated protein device has no zero-potential conductance at 300 Hz. Fig. 12B demonstrated the presence of quantum conductance of the innate protein device at 10 kHz which is based on Fig. 4C the first scan cycle. The activated device is 80.6-fold higher in the differential conductance density than the innate protein device at 10 kHz. It confirmed the fact that the large and small "donuts" or toroidal rings' alignment in the superlattice promotes the cooper pairs' hopping with the holes at the junction tunnel for the Biomimetic device at relatively lower potential than the protein device in the innate and activated states.

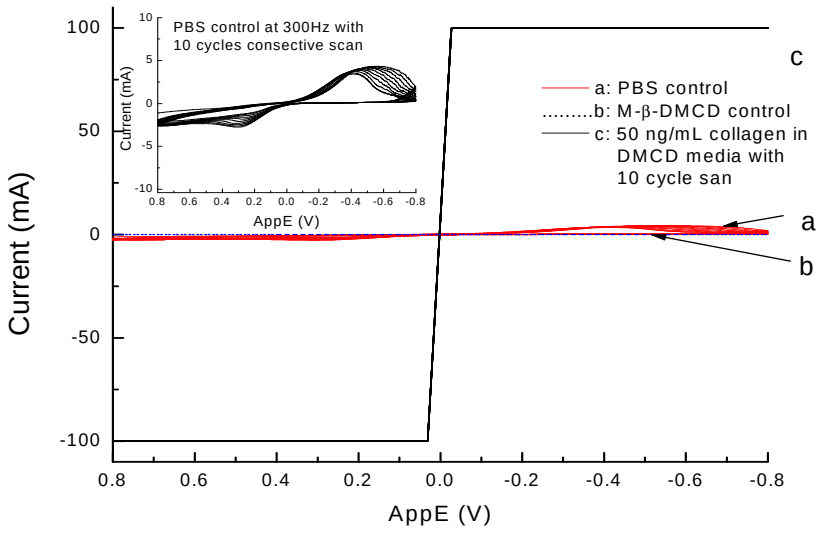

Fig. 11A. Biomimetic device's superconductivity in PBS in the presence of collagen-1 and MCD compared with the controls.

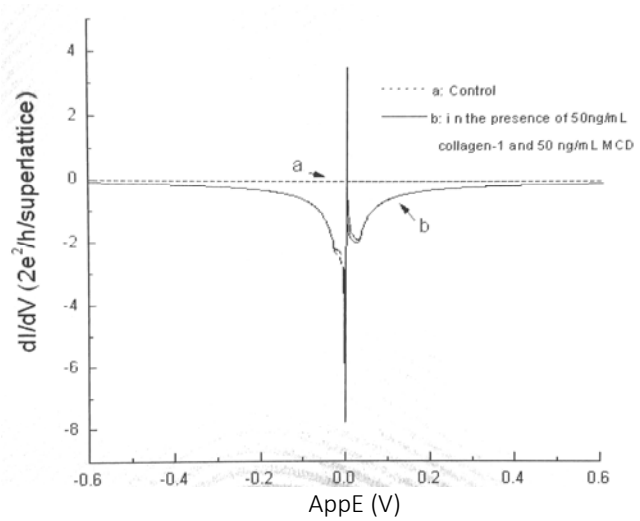

Fig. 11B. The dI/dV quantum conductance density curves in the two situations.

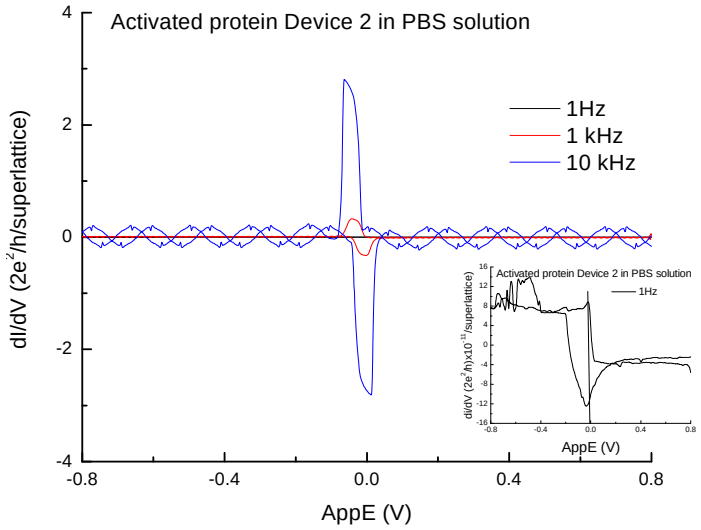

Fig. 12A. Zero-bias differential conductance density curves from activated protein device in the 10 mM PBS solution at 1 Hz, 1 kHz and 10 kHz scan rate with the insert at 1 Hz.

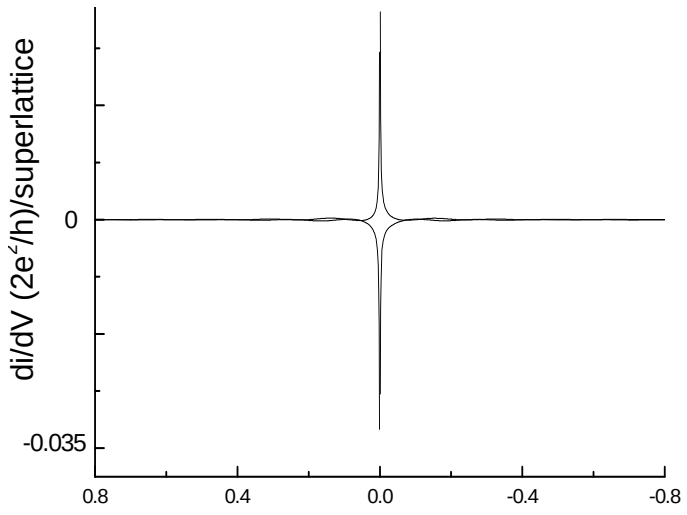

Fig. 12B. Zero-bias quantum differential conductance density curves from the innate protein device in PBS solution at 10 kHz scan rate of the first scan cycle in Fig. 4C.

6. Sensing and Quantitation of Collagen-1

6.1. The CV Method

Fig. 13A depicts the i-V curves of the Biomimetic device's direct measurement of collagen-1 over 0.5 pg/mL to 5 ng/mL compared with the control in PBS solution. Fig. 13B depicts an exponential decay relationship between the DET_{ox} peak current and the collagen concentration in PBS solution.

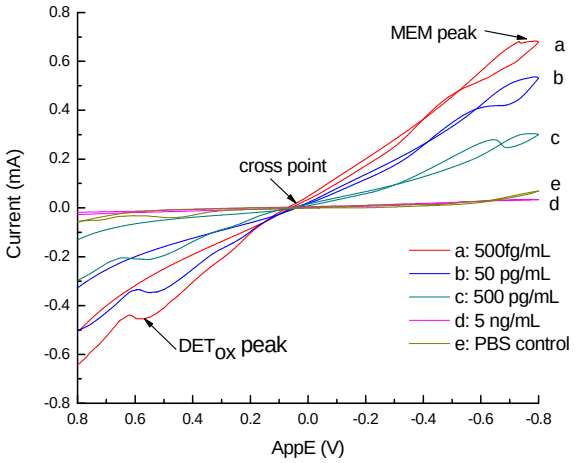

Fig. 13A. i-V curves of the memristive characteristics of Device 1 in PBS in the presence of collagen-1 over 0.5 pg/mL to 5 ng/mL vs. control at 200 Hz scan rate.

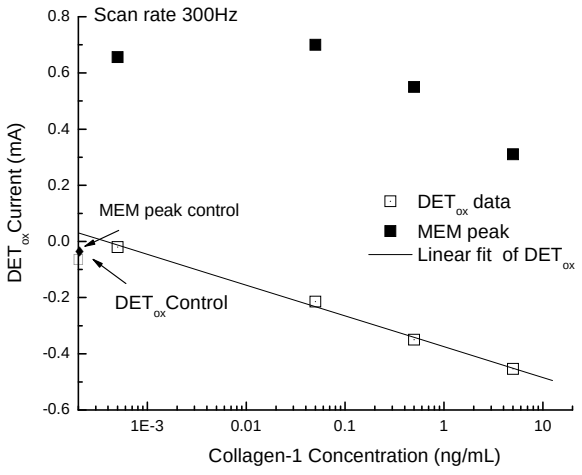

Fig. 13B. Depicts Device 1's DET_{ox} peak current vs. collagen-1 concentrations in a log scale. The solid squire represents MEM peaks.

The biomimetic device has 1.2×10^{7}-fold increase in detection sensitivity and testing range compared with protein device at the innate state as shown in Fig. 14A of the i-V profiles and Fig. 14B of the calibration curve. However, it was shown the first time that the native MMP-2 innate sensor can directly sense the presence of collagen-1 in 0.5 pg/mL to 0.5 ng/mL linearly without denaturing and without labeling, and that is due to the toroidal superlattice structure of the membrane, which stimulates the localized biological zinc atoms to become mobile and causes the Friedel-oscillation with function groups in collagen-1 and in the polymers. Fig. 14C depicts that the activated protein device communicates with collagen-1 in a superconducting way upon increased concentration. There is an inverted relationship between the concentration and the JJ current; while the location of the peak observed is closer at the zero-voltage trajectory using human capillary blood serum when concentration increased from 50 pg/mL to 100 ng/mL at 300 Hz.

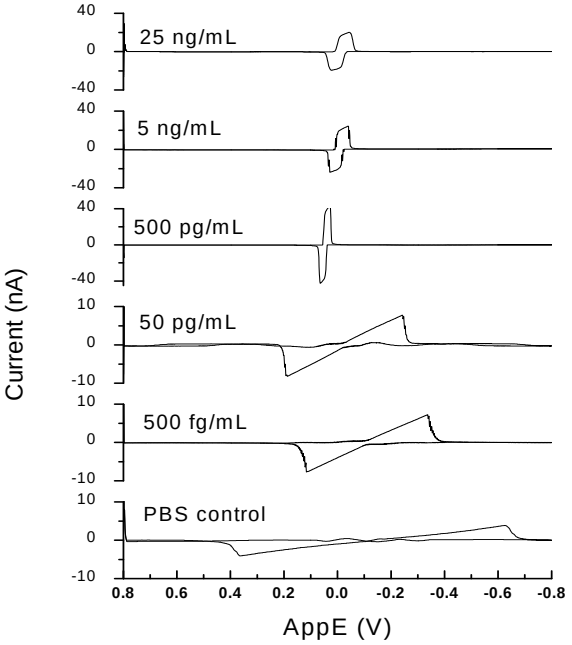

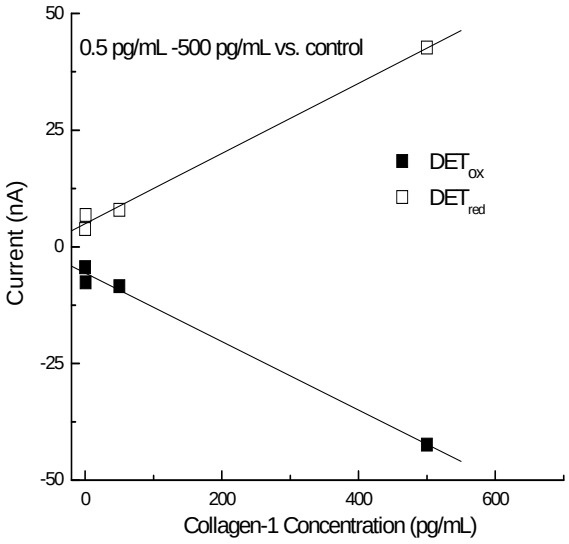

Fig. 14. A. i-V plots of the innate protein device with or w/o collagen-1 in PBS at 300 Hz. **B.** Linear plots of current vs. collagen-1 concentrations for DET_{red} and DET_{ox} peaks over 0.5 pg/mL to 500 pg/mL, respectively.

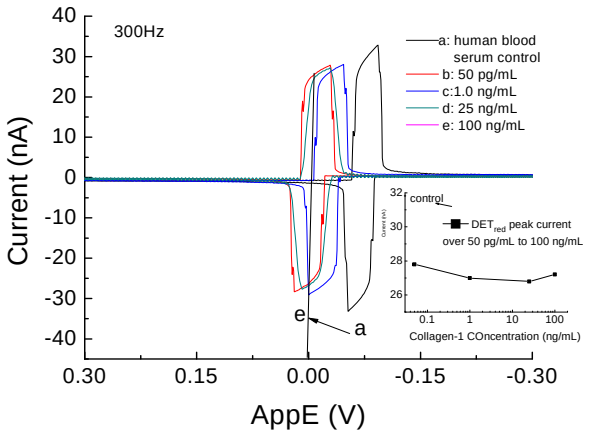

Fig. 14C. CV profiles of the activated protein device with or w/o spiking collagen-1 in human capillary blood serum.

6.2. The CA Method

Fig. 15A depicts the curves of current vs. time under -0.3 V over collagen-1 concentrations 5.0 fg/mL to 200 ng/mL compared with the control in PBS solution. Inserts are the enlarged view of the profiles at low and high levels, respectively. All curves oscillating at the AC JJ were observed. Fig. 15(A) depicts the linear regression calibration curve of current density vs. collangen-1 concentrations over the linear range of 5.0 fg/mL to 100 ng/mL (6 levels) with the regression equation y = 0.46 + 0.094x, r = 0.997, Sy/x = 0.299, p<0.0001. Fig. 15(B) depicts the biomimetic device's exponential current vs. concentration curve over 5.0 fg/mL to 200 ng/mL (9 levels) with a Detection of Limits (DOL) of 0.43 pg/mL/cm^2 (14 fg/mL for this sensor) with a relative percent of sum of squares pure error (RSSPE) of 0.05 % at the high end and 0.5 % at the low end, respectively.

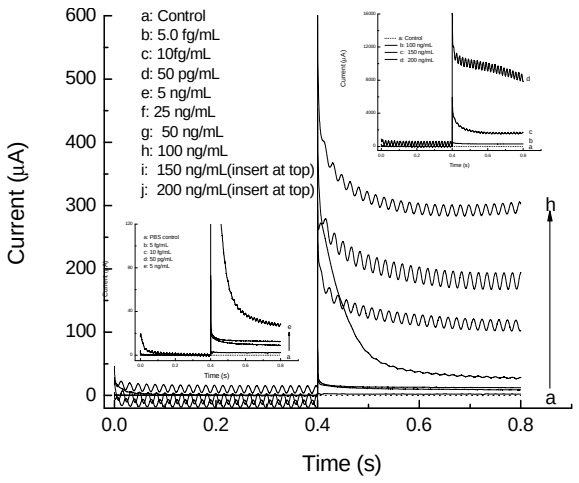

Fig. 15A. Biomimetic device's current profiles over collagen level 5.0 fg/mL to 200 ng/mL (9 levels) vs. controls in the PBS solution. Samples run triplicates. Inserts are for the enlarged view for the results at high and low end concentration levels compared with controls.

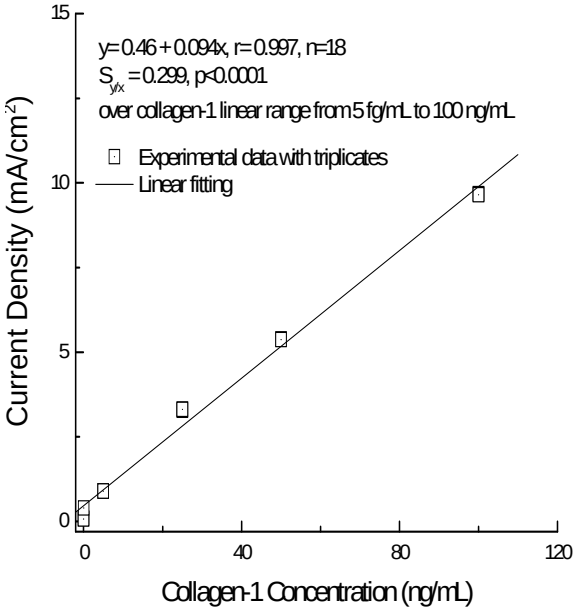

(A)

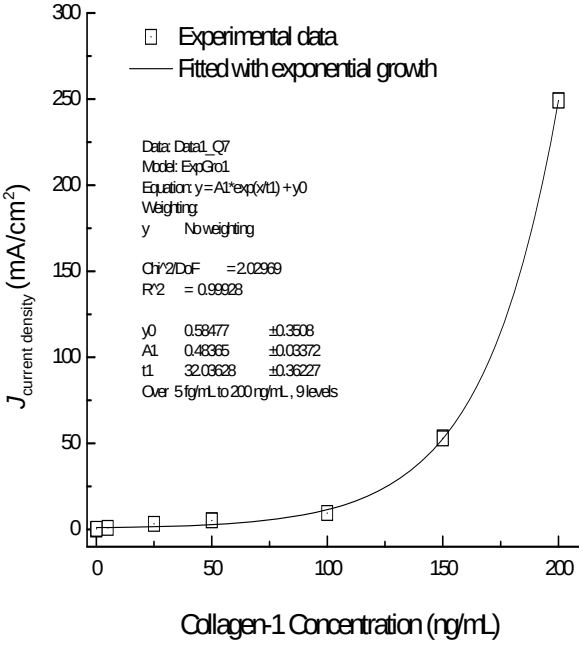

(B)

Fig. 15. (A) Calibration curve of current density vs. collangen-1 concentrations over the linear range over 5 fg/mL to 100 ng/mL (6 levels). **(B)** Exponential calibration curve over 5.0 fg/mL to 200 ng/mL (9 levels).

6.3. Point Accuracy and Imprecision

Point accuracy and imprecision was studied through the recovery experiments using spiked human fresh finger capillary blood (CPWB) serum specimens as controls spiked with 2 levels of collagen concentrations over 2.5 pg/mL to 166 ng/mL, and we compared the measured results

with the calibration curve after subtraction of the currents from control serum samples. The recovery results were 96.4± 3.4 % and 97.9 ± 0.73 % with an imprecision of 4.9 % and 0.8 % at 2.5 pg/mL and 166 ng/mL level, respectively by the CA method. Due to the strong wave oscillation occur in both the PBS solution and the finger serum, Device 2 at both the innate and activated states was unable to respond to concentration changes of collagen-1 from 500 fg/mL to 100 ng/mL both in PBS and in human finger serum using the CA method under the fixed potential.

7. Experimental

The Biomimetic MMP-2 device was freshly prepared with two steps: first, by the self-assembling method with compositions of triacetyl-ß-cyclodextrin (TCD), polyethylene glycol diglycidyl ether (PEG), poly(4-vinylpyridine) (PVP) and β-cyclodextrin copolymer (β-CD) as a mixture with appropriate proportions and forming nano island layer 1 that mimics CHAT on a 50 nm gold chip at 35°C for 48 hrs. Second, after a washing and drying process, we deposit the second polymer mixture of bis-substituted dimethyl-β-cyclodextrin (bM-β-DMCD)/TCD/PEG/PVP and embed it with zinc chloride on the top of the first layer. For the first 2 hours, the temperature was kept at 80°C. After that, the temperature was reduced to 37°C for 96 hours. Other washing and dry procedures we used were based on the literature [9]. Procedures of synthesis and characterization of mM-β-DMCD and bM-β-DMCD were based on the published literature [20]. The protein device was fabricated using the polymer mixture of TCD/PVP/PEG and native MMP-2 protein in appropriate proportions at 37°C for 96 hours on a gold chip.

The morphology of the AU/SAM was characterized using an Atomic Force Microscope (AFM) (model Dimension Edge AFM, Bruker, MA). Data collected in TappingMode using silicon probes with 5-10 nm tip radius and ~300 kHz resonance frequency (Probe mode TESPA-V2, Bruker, MA).

8. Conclusion

We demonstrated the superconductive// memristive device promotes superconductivity and memristivity, its quantum conductance density per superlattice is 3.1×10^{10}, 13 and 1.33-fold higher than that of activated protein device at 1 Hz, 1 kHz and 10 kHz, respectively, and its ability to direct detection of sub fg/mL collagen -1 with higher sensitivity and wider range compared with Device 2 at innate and activated states was also demonstrated. We also reported the ability of the innate Device 2 to direct sense 0.5 pg/mL to 500 pg/mL collagen-1 without denaturing procedures. The superconductive/ memristive technology having external magnetic field-free conditions and working at the room temperature may find broad applications in various areas in the future.

9. Conclusions and Discussions

Superconductive/memristive devices developed based on a protein Matrix Matelloproteinase-2 (MMP) cross-linked polymer toroidal membrane and a biomimetic double-layered superlattice organo-metalic membrane have shown the advantages in superconductivity, direct sensing and memristivity. Cooper pair's two-wave sounds were "heard" in the Josephson toroidal junction using the Open Circuit Potential method. It provided the first-hand knowledge and results for further study of the Cooper pair activities. The rate constant for the exponential voltage decay curve of the innate protein device is 122-fold higher than that of the biomimetic device, i.e., the protein device has 0.57s for the half-life in the JJ location compared with the double-layered biomimetic device, which has a longer half-life of 66.63s stayed in the junction for enhanced the capability for nonvolatile memory storage. Sine wave phase change and oscillating curves were observed at 1 and 10 kHz for multiple scan cycles, with peak intensity kept constant on the innate protein device compared with the biomimetic device. Because the second wave "sound" was randomly happened, therefore more advanced technology is needed for further explode in this area. All waves in the increase potential state were repeatable for the two devices, but the waves in decrease potential happened in our lucky state. The quantum conductance density of the biomimetic device is 3.1×10^{10}-fold higher than the activated protein device at 1 Hz. The protein devices were able to direct detect collagen -1 at the innate and activated state. The biomimetic device has a wider analytical range and higher sensitivity compared with the protein device.

Acknowledgements

We thank the NIST NanoLab for the clean room, the PDMS Lab and equipments used to fabricate the sensors. E. Chen thanks Dr. Richard Kasica's help and his valuable discussions.

References

[1]. J. K. Kular, S. Basu, R. I. Sharma, The extracellular matrix: structure, composition, age-related differences, tools for analysis and applications for tissue engineering, *J. Tissue Engineering*, Vol. 5, 2014, pp. 1-17.

[2]. T. Watanabe-Nakayama, M. Itami, N. Kodera, *et al*., High-speed atomic force microscopy reveals strongly polarized movement of clostridial collagenase along

collagen fibrils, *Scientific Reports*, Vol. 6, 2016, 28975.
[3]. M. F. Najafi, S. Zahri, F. Vahedi, *et al*., Which form of collagen is suitable for nerve cell culture ? *Neural Regeneration Research*, Vol. 8, Issue 23, 2013, pp. 2165-2170.
[4]. W. McKleroy, T.-H. Lee, K. Atabai, Always cleave up mess: targeting collagen degradation to treat tissue fibrosis, *Am J Physiol Lung Cell Mol Physiol*, Vol. 304, Issue 11, 2013, pp. L709-L721.
[5]. E. Takai, K. D. Costa, A. Shaheen, *et al*., Osteoblast elastic modulus measured by atomic force microscopy is substrate dependent, *Annals of Biomedical Engineering*, Vol. 33, Issue 7, 2005, pp. 963-971.
[6]. B. H. San, Y. Li, E. B. Tarbet, S. M. Yu, Nanoparticle assembly and gelatin binding mediated by triple helical collagen mimetic peptide, *ACS Applied Materials and Interfaces*, Vol. 8, Issue 31, 2016, pp. 19907-19915.
[7]. E. Seo, K. W. Seo, J.-E. Gil, Y.-R. Ha, *et al*., Biophysiochemical properties of endothelial cells cultured on bio-inspired collagen films, *BioMed Central Biotechnology*, Vol. 14, 2014, 61.
[8]. E. Wolf, G. Arnold, M. Gurvitch, J. Zasadzinski, Josephson Junctions, History, Devices, and Applications, *Pan Stanford Publishing Pte. Ltd*., 2017.
[9]. S. Frolov, Quantum Transport, www.sergeyfrolov.wordpress.com/teaching
[10]. S. Kivelson, Superconductivity and Quantum Mechanics at Micro – Scale, Stanford University. http://www.youtube.com/watch?v=yx666k2xH8E
[11]. E. Grosfeld, A. Stern, Observing Majorana bound states of Josephson vortices in topological superconductors, *PNAS*, Vol. 108, Issue 29, 2011, pp. 11810-11814.
[12]. X. Liu, X. Li, D-L. Deng, X-J. Liu, S. Das Sarma, Majorana Spintronics, *Phys. Rev. B*, Vol. 94, Issue 1, 2016, pp. 014511-014523.
[13]. J. Li, T. Neupert, B. A. Bernevig, A. Yazdani, Manipulating Majorana zero modes on atomic rings with an external magnetic field, *Nature Communications*, Vol. 7, 2016, 10395.
[14]. E. T. Chen, J. T. Thornton, P. T. Kissinger, S.-H. Duh, Nanobiomimetic Structured Superconductive/Memristive Organo-Metal Devices at Room Temperature Serve as Amperometric Sensors for sub fg/mL Collagen-1, *Biotech, Biomaterials and Biomedical TechConnect Briefs*, 2018, pp. 107-110.
[15]. E. T. Chen, J. T. Thornton, P. T. Kissinger, S.-H. Duh, Discovering of Collagen-1's Role in Producing Superconducting Current in Nanobiomimetic Superlattice Structured Organometallic Devices at Room Temperature Enabled Direct Quantitation of Sub pg/mL Collagen-1, *TechConnect Briefs*, in Informatics, Electronics and Microsystems, 2018, pp. 43-46.
[16]. J. Salmileto, F. Deppe, M. Di Ventra, Quantum memristors with superconducting circuits, *Scientific Reposrts*, Vol. 7, 2017, pp. 1-6, 42044.
[17]. C. Guarcello, P. Solinas, M. Di Ventra, F. Giazotto, *Scientific Reports*, Vol. 7, Article number: 46736, 2017.
[18]. M. Ternes, M. Pivetta, F. Patthey, W.-D. Schneider, Creation, electronic properties, disorder, and melting of two-dimensional surface-state-mediated adatom, *Progress in Surface Science*, Vol. 85, 2010, pp. 1-27.
[19]. E. T. Chen, H. L. Pardue, Analytical applications of catalytic properties of modified cyclodextrins, *Anal. Chem*, Vol. 65, Issue 19, 1993, pp. 2583-2587.
[20]. M. D. Pickett, G. Medeiros-Ribeiro, R. S. Williams, A scalable neuristor built with Mott memristors, *Nature Materials*, Vol. 12, Issue 2, 2013, pp. 114-117.
[21]. J. E. Redman, Solution, surface and solid state assembly of porphyrins, *University of Cambridge*, 2000.
[22]. R. V. Slone, J. T. Hupp, Synthesis, characterization, and preliminary host-guest binding studies of porphyrinic molecular squares featuring fac-tricarbonylrhenium(1) chloro corners, *Inorg. Chem*, Vol. 36, Issue 24, 1997, pp. 5422-5672.
[23]. M. S. Liao, Electronic structure and bonding in metal porphyrins, metal=Fe, Co, Ni, Cu, Zn, *Journal of Chemical Physics*, Issue 117, Issue 1, 2002, pp. 205-219.
[24]. S. Davari, S. A. Talaei, H. Alaei, M. Salami, Probiotics treatment improves diabetes induced impairment of synaptic activity and cognitive function: behavioral and electrophysiological proofs for microbiom-gut-brain axis, *Neuroscience*, Vol. 240, 2013, pp. 287-296.

Published by International Frequency Sensor Association (IFSA) Publishing, S. L., 2018 (http://www.sensorsportal.com).